NMR, UV-Visible, NLO, NBO, MEP and Vibrational Spectroscopic (IR and Raman) Analysis of O-Nitrobenzamide

- Rev. Fr. S. Xavier[*]
- S. Sumathi[**]
- K. Sivakamasundari [***]

Abstract

In the present methodical study, FT-IR, FT-Raman and NMR spectra of o-nitrobenzamide are recorded and the fundamental vibrational frequencies are tabulated and assigned. The vibrational wavenumbers were computed using HF and DFT methods and are assigned with the help of potential energy distribution method. Gaussian hybrid computational calculations are carried out using HF and DFT (B3LYP and B3PW91) methods with 6-31+G (d,p) and cc-pVDZ & aug-cc-pVDZ basis sets. Moreover, ^{1}H and ^{13}C NMR spectra have been analysed and ^{1}H and ^{13}C nuclear magnetic resonance chemical shifts are calculated using the gauge independent atomic orbital (GIAO) method. A study on the electronic and optical properties (absorption wavelengths, excitation energy, dipole moment and frontier molecular orbital energies) is performed using HF and DFT methods. Stability of the molecule arising from hyper conjugative interactions, charge delocalization has been analysed using natural bond orbital (NBO) analysis. The calculated HOMO and LUMO energies (kubo gap) are displayed in the figures, which show the occurrence of charge transformation within the molecule. Besides frontier molecular orbital (FMO) energy, molecular electrostatic potential (MEP) was also calculated. NLO properties related to polarizability and hyperpolarizability are also discussed. The local reactivity of the molecule has been studied using the Fukui function.

Keywords: o-nitrobenzamide; gauge-independent atomic orbital; chemical shifts; FMO, Fukui function.

Introduction

O-nitrobenzamide is an organic compound, which consists of nitro; carbonyl and amide groups are attached to the phenyl ring. It reacts with azo and diazo compounds to generate toxic gases. Flammable gases are formed by the reaction of O-nitrobenzamide with strong reducing agents. O-nitrobenzamide has very weak bases (weaker than water). These derivatives are less basic yet and in fact react with strong bases

[*]Department of Physics, St. Joseph's College of Arts and Science (Autonomous), Cuddalore, Tamil Nadu, India.
[**]Department of Physics, St. Joseph's College of Arts and Science (Autonomous), Cuddalore, Tamil Nadu, India.
[***] Research Scholar, Bharathiyar University, Coimbatore.

to form salts. That is, they can react as acids. Mixing amides with dehydrating agents such as P_2O_5 or $SOCl_2$ generate the corresponding nitrile. The combustion of these compounds generates mixed oxides of nitrogen (NOx). It is a stable compound and does not undergo polymerization. O-nitrobenzamide is easily oxidized by using Strong oxidizing agents. Exposure to air or moisture over prolonged periods destroys the nature of the amide.

The IUPAC name of O-nitrobenzamide is 2-Nitrobenzamide. The molecular formula of O-nitrobenzamide is $C_7H_6N_2O_3$ and the molecular weight is 166.13. It is a kind of beige crystalline powder and belongs to the classes of Aromatic Carboxylic Acids, Amides, Anilides and Carbonyl Compounds; Organic Building Blocks. Other synonyms of o-nitrobenzamide are: 2-Nitrophenylformamide;benzamide, o-nitro-;2-Carbamoylnitrobenzene.

Preparation of 2-Nitrobenzamide

It can be prepared by the reaction 2-nitro-benzonitrile with Al_2O_3 and $MeSO_3H$. The reaction time is 15 minutes at reaction temperature of 120 °C. The yield is about 90%.

2-nitrobenzonitrile → 2-nitrobenzamide (Al₂O₃ / MeSO₃H, 120 °C)
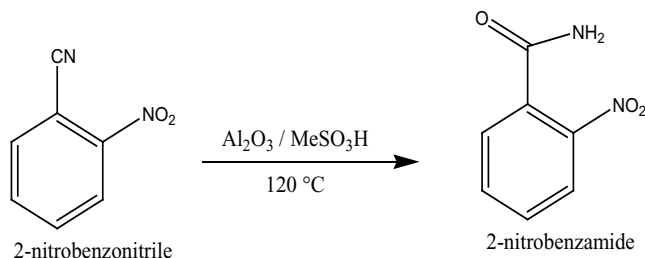
Applications

2-Nitrobenzamide was used in the synthesis of novel fluorogenic chemosensors based on urea derivative of 2-(2′-aminophenyl)-4-phenylthiazole. It was also used in the synthesis of quinazoline-2,4(1*H*,3*H*)-diones, an important class of pharmaceutical intermediates[1].

There is provided 5-(aziridin-1-yl)-4-hydroxylamino-2-nitrobenzamide for various uses, as well as pharmaceutical compositions and devices comprising 5-(aziridin-1-yl)-4-hydroxylamino-2-

nitrobenzamide [2]. There are also other methods provided for reducing reducible compounds (such as reduction-activated prodrugs, e.g. tretazicar) by contacting those compounds with α-hydroxycarbonyl compounds capable of forming cyclic dimers.

Experimental Details

The spectra of o-nitrobenzamide are purchased from Sigma–Aldrich Chemicals, USA. The FT-IR spectrum of the compound is recorded using a Bruker IFS 66V spectrometer in the range of 4000–500 cm⁻¹. The spectral resolution is ±2 cm⁻¹. The FT-Raman spectrum of the same compound is also recorded using the same instrument with FRA 106 Raman module equipped with Nd: YAG laser source operating at 1.064 μm line width with 200 mW power. The spectra are recorded in the range of 3500–400 cm⁻¹ with a scanning speed of 30 cm⁻¹ min⁻¹ of spectral width 2 cm⁻¹. The frequencies of all sharp bands are accurate to ±1 cm⁻¹.

Computational Methods

In the present work, HF and some of the hybrid methods, B3LYP and B3PW91, are carried out using the basis sets 6-31+G (d,p) and cc-pVDZ & aug-cc-pVDZ. All these calculations are performed using the GAUSSIAN 09W [3] program package on an i7 processor in a personal computer. In DFT methods, B3LYP is the combination of Becke's three-parameter hybrid function, and the Lee–Yang–Parr correlation function [4, 5]. B3PW91 is the combination of Becke's three parameter exact exchange-function (B3) [6] and Perdew-Wang (PW91) correlation function [7, 8]. The optimized molecular structure of the molecule is obtained using the Gaussian 09 and Gaussview program and is shown in Fig. 1. The comparative optimized structural parameters such as bond length, bond angle and dihedral angle are presented in Table 1. The observed (FT-IR and FT-Raman) and calculated vibrational frequencies and vibrational assignments are presented in Table 3. Experimental and simulated spectra of IR and Raman are presented in Fig. 2 and 3, respectively.

Table 1: Optimized Geometrical Parameters of O-Nitrobenzamide

| Geometrical Parameter	HF/6-31+G (d, p)	B3LYP/ cc-pVDZ	B3LYP/ aug-cc-pVDZ	B3PW91/ cc-pVDZ	B3PW91/ aug-cc-pVDZ
Bond length(Å)					
C1-C2	1.3824	1.3965	1.3953	1.3932	1.3926
C1-C6	1.3844	1.3935	1.3947	1.3915	1.3923
C1-H7	1.0720	1.0890	1.0873	1.0896	1.0880
C2-C3	1.3885	1.4019	1.4020	1.3988	1.3989
C2-N16	1.4608	1.4787	1.4766	1.4726	1.4707
C3-C4	1.3878	1.4020	1.4012	1.3992	1.3986
C3-C11	1.5149	1.5229	1.5171	1.5181	1.5133
C4-C5	1.3873	1.3966	1.3977	1.3946	1.3953
C4-H8	1.0747	1.0915	1.0896	1.0916	1.0901
C5-C6	1.3853	1.3987	1.3980	1.3961	1.3957
C5-H9	1.0750	1.0921	1.0901	1.0921	1.0905
C6-H10	1.0743	1.0914	1.0895	1.0914	1.0899
C11-N12	1.3538	1.3695	1.3671	1.3650	1.3633
C11-O15	1.1949	1.2165	1.2201	1.2148	1.2182
N12-H13	0.9963	1.0170	1.0123	1.0157	1.0115
N12-H14	0.9939	1.0145	1.0101	1.0133	1.0094
N16-O17	1.1921	1.2234	1.2268	1.2180	1.2213
N16-O18	1.1947	1.2273	1.2287	1.2214	1.2230
Bond angle(°)					
C2-C1-C6	119.0509	119.2607	119.1608	119.2364	119.1441
C2-C1-H7	119.5570	118.6869	119.1169	118.6622	118.9830
C6-C1-H7	121.3899	122.0522	121.7189	122.1009	121.8694
C1-C2-C3	122.3741	122.2871	122.2790	122.3120	122.3125
C1-C2-N16	117.5141	117.4046	117.5516	117.5037	117.5828
C3-C2-N16	120.0770	120.2823	120.1418	120.1508	120.0768
C2-C3-C4	117.6526	117.3564	117.5168	117.4108	117.5295
C2-C3-C11	124.1230	124.7048	124.0137	124.3306	123.9706
C4-C3-C11	117.9677	117.5738	118.1082	117.8762	118.1485
C3-C4-C5	120.8002	121.1327	120.982	121.0648	120.9504
C3-C4-H8	119.1754	118.7378	118.9565	118.7821	118.9345
C5-C4-H8	120.0145	120.1274	120.0516	120.1499	120.1057
C4-C5-C6	120.3813	120.272	120.281	120.2896	120.2985
C4-C5-H9	119.56	119.6414	119.6301	119.634	119.6228
C6-C5-H9	120.057	120.0853	120.0873	120.075	120.0772
C1-C6-C5	119.7332	119.6853	119.7707	119.6804	119.755
C1-C6-H10	119.7764	119.8309	119.7817	119.832	119.7955
C5-C6-H10	120.4902	120.4837	120.4475	120.4874	120.4493
C3-C11-N12	115.2722	114.8585	115.3178	114.6749	115.1494
C3-C11-O15	120.5307	120.5118	120.5817	120.5567	120.5548
N12-C11-O15	123.875	124.1315	123.7072	124.2923	123.8866
C11-N12-H13	115.8144	114.7257	116.3293	115.0125	116.2744
C11-N12-H14	119.3354	117.48	119.5092	117.7549	119.283
H13-N12-H14	116.7363	115.3259	117.0742	115.6925	117.0798
C2-N16-O17	117.7678	117.7686	117.8141	117.6843	117.7303
C2-N16-O18	117.0905	117.2884	117.3545	117.1495	117.2526
O17-N16-O18	125.1204	124.9316	124.8163	125.1525	125.0022
Dihedral Angle(°)					
C6-C1-C2-C3	-1.0091	-0.697	-1.1373	-0.7658	-1.1555
C6-C1-C2-N16	176.8431	177.4508	176.9525	177.1293	176.9215
H7-C1-C2-C3	179.5178	179.464	179.5239	179.4799	179.5107
H7-C1-C2-N16	-2.63	-2.3882	-2.3863	-2.6251	-2.4122
C2-C1-C6-C5	0.3858	0.3084	0.4541	0.2925	0.4699
C2-C1-C6-H10	-179.5073	-179.5693	-179.4038	-179.541	-179.3868
H7-C1-C6-C5	179.849	-179.8582	179.7749	-179.9619	179.7837
H7-C1-C6-H10	-0.0442	0.2641	-0.083	0.2046	-0.0731
C1-C2-C3-C4	0.936	0.3534	0.9839	0.5015	0.9811
C1-C2-C3-C11	-173.1128	-172.522	-171.9698	-172.2309	-172.0716
N16-C2-C3-C4	-176.8628	-177.7424	-177.0577	-177.3393	-177.0493

N16-C2-C3-C11	9.0885	9.3822	9.9886	9.9283	9.898
C1-C2-N16-O17	25.5148	16.9002	22.4557	18.5233	21.9369
C1-C2-N16-O18	-152.8936	-161.9383	-156.197	-160.1976	-156.729
C3-C2-N16-O17	-156.5814	-164.913	-159.4117	-163.534	-159.9411
C3-C2-N16-O18	25.0102	16.2485	21.9355	17.7451	21.393
C2-C3-C4-C5	-0.2555	0.3737	-0.1662	0.2273	-0.1396
C2-C3-C4-H8	-179.1085	-179.0928	-179.017	-179.13	-179.0241
C11-C3-C4-C5	174.1676	173.7685	173.2141	173.4402	173.3278
C11-C3-C4-H8	-4.6854	-5.6981	-5.6367	-5.917	-5.5566
C2-C3-C11-N12	-111.2264	-101.7148	-111.742	-105.3585	-111.4727
C2-C3-C11-O15	75.0428	86.0545	75.1947	82.226	75.5901
C4-C3-C11-N12	74.7422	85.4239	75.3431	81.9403	75.5146
C4-C3-C11-O15	-98.9886	-86.8067	-97.7202	-90.4753	-97.4226
C3-C4-C5-C6	-0.3305	-0.7522	-0.4788	-0.6837	-0.5075
C3-C4-C5-H9	-179.8526	179.6711	179.9806	179.7412	179.9487
H8-C4-C5-C6	178.5129	178.707	178.3595	178.6648	178.3639
H8-C4-C5-H9	-1.0092	-0.8697	-1.1811	-0.9102	-1.1799
C4-C5-C6-C1	0.2655	0.3992	0.3329	0.415	0.3397
C4-C5-C6-H10	-179.8422	-179.7239	-179.8101	-179.7526	-179.8045
H9-C5-C6-C1	179.7852	179.9739	179.8713	179.9881	179.8814
H9-C5-C6-H10	-0.3225	-0.1492	-0.2717	-0.1794	-0.2628
C3-C11-N12-H13	173.1876	171.3074	174.0636	171.4957	173.7856
C3-C11-N12-H14	25.5031	30.9223	24.3394	29.67	24.5916
O15-C11-N12-H13	-13.3175	-16.781	-13.1163	-16.4116	-13.5424
O15-C11-N12-H14	-161.002	-157.1661	-162.8405	-158.2373	-162.7364

Table 2: Observed and Calculated Vibrational frequencies of O-Nitrobenzamide Using HF and DFT (B3LYP & B3PW91) at the 6-31+G(d, p) & cc-pVDZ, aug cc-pVDZ Basic Sets

S. No.	Observed Frequency(cm^{-1})		Methods					Vibrational Assignments
			HF	B3LYP		B3PW91		
	FT-IR	FT Raman	6-31+G (d, p)	cc-pVDZ	aug-cc-pVDZ	cc-pVDZ	aug-cc-pVDZ	
1	3390 vs	-	3512	3494	3535	3496	3532	υN-H (100%)
2	3390 vs	-	3392	3372	3408	3370	3403	υN-H (100%)
3	3100 s	-	3034	3087	3094	3071	3079	υC-H (95%)
4		3090 m	3008	3062	3071	3050	3060	υC-H (97%)
5		3080m	2999	3053	3062	3040	3050	υC-H (97%)
6		3050m	2987	3041	3051	3028	3039	υC-H (100%)
7	1680 vs	-	1744	1720	1683	1724	1692	υC=O (84%)
8	1600 s	-	1639	1596	1585	1608	1595	υN=O (31%) + υC=C (36%)
9	1590 w	-	1591	1559	1551	1570	1561	υN=O (35%) + υC=C (33%)
10	1580 w	-	1672	1646	1647	1652	1646	υN=O (12%) + υC-C (43%)
11	-	1570 vw	1654	1628	1629	1615	1632	δNH$_2$ (74%)
12	1520 vs		1556	1532	1531	1527	1525	υC-C (14%) + δHCC (48%)
13	1470 m	-	1538	1490	1485	1483	1478	υC-C (13%) + δHCC (44%)
14	1430 w	-	1501	1423	1419	1443	1438	υN=O (77%) + δONO (10%)
15	1400 m	1400 vw	1396	1391	1391	1403	1397	υN-C (30%) + υC=C (18%) + δHNC (13%) + δNCO (12%)
16	1400 m	1400 vw	1322	1388	1383	1393	1393	υC-C (78%)
17	1320 w	-	1255	1298	1303	1287	1291	δHCC (58%)
18	1270 w	1270 vw	1194	1196	1202	1191	1194	δHCC (67%)
19	1230 vw	-	1178	1271	1275	1280	1282	υC=C (17%) + υN-C (10%) + δHCC (29%)
20	1230 vw	-	1223	1257	1261	1261	1264	υC=C (15%) + δHNC (12%) + δHCC (24%)
21	1230 vw	-	1215	1216	1211	1218	1211	υO=C (12%) + υN=C (27%) + δHNC (42%)
22	1180 vw	-	1180	1184	1184	1156	1187	υN-C (12%) + δCCC (45%)
23	1130 m	-	1133	1157	1160	1163	1164	υC=C (71%) + δHCC (12%)
24	1130 m	-	1132	1109	1107	1108	1098	τHCCN (14%) + τHCCC (66%)
25	1090 vw	-	1100	1074	1070	1073	1067	τHCCN (40%) + τHCCC (42%)
26	1000 vw	1000 vw	1003	983	979	982	977	τHCCN (27%) + τHCCC (50%)
27	970 vw	970 vw	963	952	949	962	957	υN-C (10%) + γCCC (14%) + γOCN (47%)
28	890 vw	890 vw	899	875	879	878	882	τHCCC (54%) + γOCON (30%)
29	860 m	860 vw	859	844	849	844	849	γOCON (10%) + γHCC (50%)
30	850 vw	850 vw	838	833	835	833	834	δCCC (22%) + γOCNC (33%)
31	830 vw	-	823	828	824	829	825	γOCNC (27%) + γNH$_2$
32	790 m	790 vw	785	778	780	780	781	τHCCC (11%) + τCCCC (25%) + γOCON (36%)

33	730 w	730 vw	728	741	739	741	740	υN-C (11%) + γCCC (29%) + γONO (18%)
34	665 w	-	661	670	668	666	665	γNCO (40%) + γCCC (11%)
35	620 vw	-	617	631	626	629	625	τHNCC (38%)
36	600 vw	-	611	620	620	618.6	619	γCCN (21%) + τHNCC (14%) + τCCCC (13%)
37	570 vw	570 vw	567	1569	1368	1530	1368	γCNO (25%) + τHNCC (30%)
38	-	470 vw	467	1327	1128	1288	1123	τHNCC (76%)
39	-	440 vw	455	1265	1094	1224	1097	τCCCC (33%) + γNCCC (23%)
40	-	430 vw	1243	1218	1078	1193	1081	υN-C (30%) + γCCC (13%)
41	-	390 vw	1071	1038	930	1008	923	γCCN (20%) + τCCCC (52%)
42	-	360 vw	971	943	851	924	847	υC=C (15%) + γCNO (11%) + γCCC (17%) + γCCN (13%)
43	-	360 vw	788	775	685	752	681	γCNO (14%) + γCCN (46%)
44	-	360 vw	516	504	440	486	439	γCCC (12%) + γNCCC (24%) + γCCCC (22%)
45	-	360 vw	469	468	406	446	399	γCCC (44%) + γCCN (13%)
46	-	360 vw	333	309	276	299	276	τCCCC (41%) + γCCCC (32%)
47	-	360 vw	255	194	208	207	213	τCCNO (63%) + τCCCN (21%)
48	-	360 vw	103	73	84.37	74.91	84	τCCNO (21%) + τCCCN (65%)

vs – very strong, s – strong, m – medium, w – weak, vw – very weak

υ-stretching, δ-in-plane bending, γ-out-of-plane bending, τ-torsional
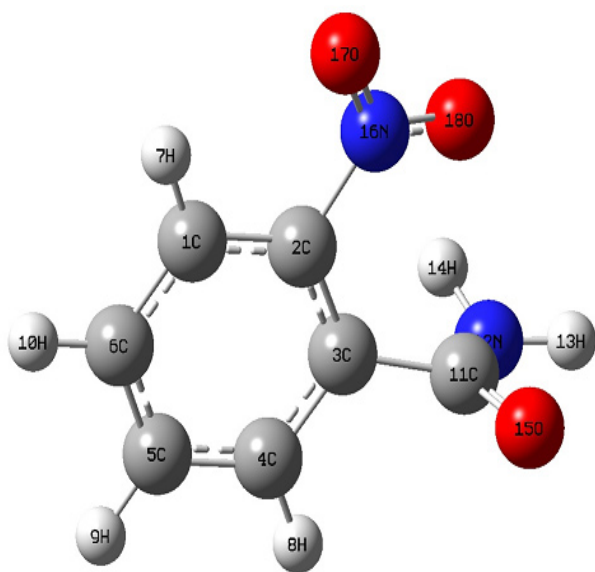
Figure 1: Molecular Structure of O-Nitrobenzamide

The ^{1}H and ^{13}C NMR isotropic shielding are calculated using the GIAO method[9] and the optimized parameters obtained from the B3LYP/cc-pVDZ method. [13]C isotropic magnetic shielding (IMS) of any X carbon atoms is made according to the ^{13}C IMS value of TMS, $CS_X = IMS_{TMS} - IMS_X$. The ^{1}H and ^{13}C isotropic chemical shifts of TMS (Tetramethylsilane) in gas, DMSO, methanol and ethanol are calculated using IEFPCM method with the B3LYP functional at the cc-pVDZ level. The absolute chemical shift is found between the isotropic peaks and the peaks of TMS [10]. Stability of the molecule arising from hyper conjugative interactions, charge delocalization is analyzed using natural bond orbital (NBO) analysis. The electronic properties, HOMO-LUMO energies, absorption wavelengths and oscillator strengths are calculated using the time-dependent DFT (TD-DFT)[11,

[12] method with the B3LYP functional in the gas phase and the solvent phase. Moreover, dipole moment, polarizability, hyperpolarizability related to nonlinear optical (NLO) properties is also studied. The local reactivity of the molecule is studied using the Fukui function. The condensed softness indices are found and are used to predict both the reactive centers and the possible sites of nucleophilic and electrophilic attack.
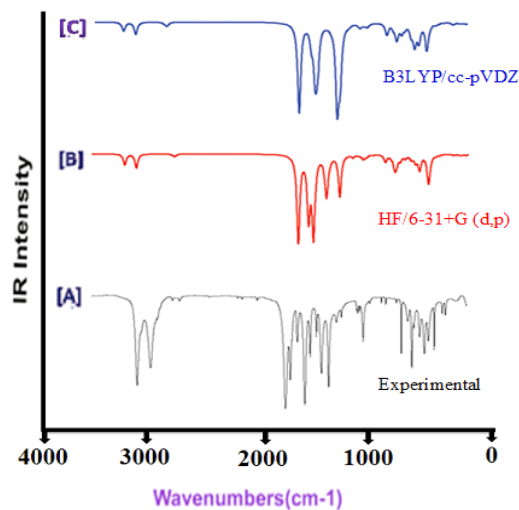
Figure 2: Experimental [A] & Calculated [B, C] FT-IR Spectra of O-Nitrobenzamide
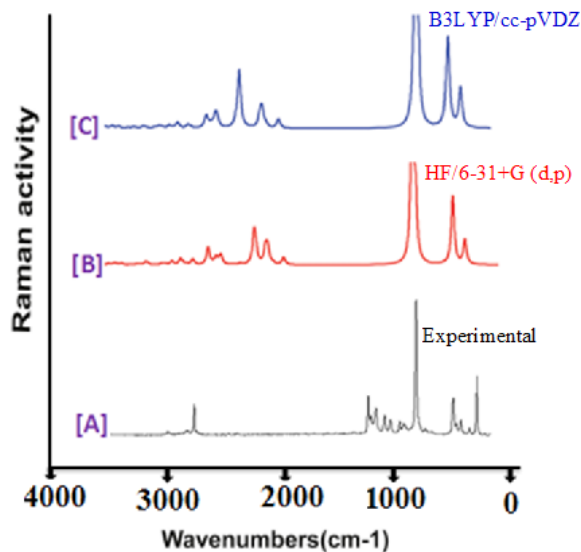
Figure 3: Experimental [A] & Calculated [B, C] FT-Raman Spectra of O-Nitrobenzamide

Results and Discussion

Molecular Geometry

From the optimized output file of Gaussian it is observed that the molecular structure of o-nitrobenzamide belongs to C_1 point group symmetry. The optimized structure of the molecule is obtained from the Gaussian 09 and Gauss view program [13] and is shown in Fig. 1. The present molecule contains one nitro group and one amide group, which are loaded in the left moiety. The hexagonal structure of the benzene is deformed at the point of substitution due to the addition of the heavy mass. It is also evident that the bond length (C1-C2 & C2-C3) at the point of substitution is 0.0054 Å, which is longer than the rest in the ring. Consequently, the property of the same also changed with respect to the ligand (nitro and amide groups). The bond angle of C1–C2–C3 is 2.0151° elevated more than C4–C5–C6 in the ring, which also confirms the deformation of the hexagonal shield. Although both C=O and NH$_2$ groups, the bond length values between C2–C3 and C3–C11 differed by 0.121 Å. The entire C–H bonds in the chain and the amide groups have almost equal inter-nuclear distance.

Table 3: Calculated unscaled frequencies of O-Nitrobenzamide using HF/DFT (B3LYP&B3PW91) with 6-31+(d,p) and cc-pVDZ, aug-cc-pVDZ basis sets

S. No.	Observed Frequency	Calculated frequency				
		HF	B3LYP		B3PW91	
		6-31+G (d, p)	cc-pVDZ	aug-cc-pVDZ	cc-pVDZ	aug-cc- pVDZ
1	3390 vs	3951	3661	3691	3693	3714
2	3390 vs	3816	3533	3558	3560	3578
3	3100 s	3413	3235	3230	3244	3237
4	3090 m	3384	3208	3206	3222	3217
5	3080 m	3374	3199	3197	3212	3207
6	3050 m	3360	3186	3185	3199	3195
7	1680 vs	1962	1802	1757	1821	1779
8	1600 s	1844	1672	1655	1699	1677
9	1590 w	1790	1633	1619	1659	1641
10	1580 w	1781	1618	1614	1635	1626
11	1570 vw	1761	1600	1596	1598	1612
12	1520 vs	1657	1506	1500	1511	1506
13	1470 m	1638	1465	1455	1468	1460
14	1430 w	1599	1399	1390	1428	1420
15	1400 m	1487	1367	1363	1388	1380
16	1400 m	1408	1364	1355	1379	1376
17	1320 w	1336	1276	1277	1274	1275
18	1270 w	1272	1176	1178	1179	1179
19	1230 vw	1255	1164	1162	1170	1169
20	1230 vw	1223	1151	1149	1153	1152
21	1230 vw	1215	1114	1103	1113	1104
22	1180 vw	1180	1084	1079	1057	1082
23	1130 m	1133	1060	1057	1063	1061
24	1130 m	1132	1016	1009	1013	1001
25	1090 vw	1100	984	975	981	973

26	1000 vw	1003	900	892	898	891
27	970 vw	963	872	865	880	873
28	890 vw	899	804	804	808	808
29	860 m	859	776	777	777	778
30	850 vw	846	766	764	767	764
31	830 vw	831	761	754	763	756
32	790 m	792	715	714	718	716
33	730 w	735	681	677	682	678
34	665 w	667	616	612	613	609
35	620 vw	623	580	573	579	573
36	600 vw	617	570	568	569	567
37	570 vw	572	532	519	531	520
38	470 vw	472	450	428	447	427
39	440 vw	459	429	415	425	417
40	430 vw	448	413	409	414	411
41	390 vw	386	352	353	350	351
42	360 vw	350	320	323	321	322
43	360 vw	284	263	260	261	259
44	360 vw	186	171	167	169	167
45	360 vw	169	159	154	155	152
46	360 vw	120	105	105	104	105
47	360 vw	92	66	79	72	81
48	360 vw	37	25	32	26	32

vs – very strong, s – strong, m – medium, w – weak, vw – very weak

Vibrational Assignments

In order to obtain the spectroscopic significance of o-nitrobenzamide, the computational calculations are performed using frequency analysis. The molecule has C_1 point group symmetry, consists of 18 atoms, so it has 48 normal vibrational modes. On the basis of C_1 symmetry, the 48 fundamental vibrations of the molecule can be distributed as 36 in-plane vibrations of A′ species and 12 out-of-plane vibrations of A″ species, i.e., Γ_{vib} = 36 A′ + 12 A″. In the C_1 group, the symmetry of the molecule is a non-planar structure and has 48 vibrational modes that span in the irreducible representations.

The vibrational frequencies (unscaled and scaled) calculated at HF, B3LYP and B3PW91methods with 6-311+G(d,p), cc-pVDZ and aug cc-pVDZ basic sets and observed FT-IR and FT-Raman frequencies for various modes of vibrations have been presented in Tables 2 and 3. The Frequencies calculated at the HF and B3LYP/B3PW91 methods are found to be high compared to experimental vibrations. The Inclusion of electron correlation in the density functional theory to a certain extent makes the frequency values smaller in comparison with the HF frequency data.

The calculated frequencies are scaled down to give up the rational with the observed frequencies. The scaling factors are 0.8889, 0.9390, 0.9999 and 0.9909 for HF/6-31+G (d, p). For the B3LYP/cc-pVDZ/aug-cc-pVDZ basis set, the scaling factors are 0.9544, 1.0174, 1.0919 and 1.0881/0.9578, 1.0207, 1.0976 and 1.0929. For the B3PW91/ cc-pVDZ/aug-cc-pVDZ basis set, the scaling factors are 0.9466, 1.0105, 1.0939 and 1.0871/0.9511, 1.0125, 1.0968 and 1.0921.

N−H, N=O Vibrations

In heterocyclic molecules, the N−H stretching vibrations have been measured in region 3500–3000 cm^{-1} [14]. As seen in Table 2, the two N−H stretching modes are calculated at 3494 and 3372 cm^{-1} in B3LYP. A very strong FT-IR N−H stretching vibration is observed at 3390 cm^{-1} in the experimental spectrum. Ten et al. [15] have observed these modes at 3479 and 3432 cm^{-1}, respectively, for isolated thymine. In 2-amino-4-methylbenzothiazole, V. Arjunan et al [16]. have observed the vibrational frequencies at 3417 and 3287 cm^{-1}. Cirak and Koc [17] have calculated the N–H stretching modes at 3189 and 3155 cm^{-1} for dimeric trifluorothymine. However, no Raman band is observed for the N−H stretching modes in the experimental spectra. For primary amino group the in-plane –NH$_2$ deformation vibration occur in the short range 1650–1580 cm^{-1} region of the spectrum. Therefore the very weak band observed in IR at 1570 cm^{-1} is assigned to the deformation mode of the amino group.

The most characteristic bands in the spectra of nitro compounds are due to NO$_2$ stretching vibrations,

which are the most useful group wavenumbers, not only because of their spectral position but also for their strong intensity [18]. The N=O stretching vibrations have been measured in region 1515-1560 cm⁻¹. A weak IR N=O stretching vibration is observed at 1430 cm⁻¹. However, no Raman band is observed for the N=O stretching modes. Hence these vibrations show good agreement with the literature values.

C–H Vibrations

The C–H stretching vibrations are normally observed in the region 3100-3000 cm⁻¹ for the aromatic benzene structure, [19–20] which shows their uniqueness of the skeletal vibrations. The bands appeared at 3100, 3090, 3080, and 3050 cm⁻¹ in o-nitrobenzamide are assigned to C–H ring stretching vibrations. The FT-IR bands at 1520 and 1470 cm⁻¹ are assigned to C–H in-plane bending vibrations and FT-IR bands at 860 cm⁻¹ are assigned to C–H out-of-plane bending vibration. V. Karunakaran et al. [21] in the molecule 4-chloro-3-nitrobenzaldehyde (CNB) have observed the bands at 3053, 3034 cm⁻¹ in FT-IR and at 3079, 3052 cm⁻¹ in FT-Raman spectra. The FT-IR bands at 1467, 1422 cm⁻¹ and the FT-Raman bands at 1423 and 1218 cm⁻¹ were assigned to C–H in-plane bending vibration of CNB. The C–H out-of-plane bending vibrations of the CNB were well identified at 989, 822 and 722 cm⁻¹ in the FT-IR and 828 cm⁻¹ in the FT-Raman spectra V. Arjunan et al. [22] in 4-acetyl benzonitrile, have been observed the C–H stretching peaks in IR at 3075 and 3030 cm⁻¹ and in Raman spectrum at 3090, 3074 and 3025 cm⁻¹. The frequencies calculated for the present compound using B3LYP/cc-pVDZ and B3LYP/aug cc-pVDZ methods for C–H in-plane bending vibrations showed excellent agreement with the recorded spectrum as well as literature data.

C–C Vibrations

V. Arjunan et al [23] in 4-acetyl benzonitrile, have observed the C–C stretching vibrations at 1593, 1556, 1485, 1415, and 1259 cm⁻¹ in IR spectrum and 1603, 1482, 1430, 1408 and 1270 cm⁻¹ in Raman spectrum. The IR bands observed at 1593 and 1285 cm⁻¹ were strong while the Raman band 1603 cm⁻¹ was very strong. In addition, C–C–C in–plane bending vibrations have been attributed to 1002 and 844 cm⁻¹ in IR spectrum and 794 cm⁻¹ in Raman spectrum. The C–C–C out of plane vibrations have been observed at 337, 227 and

108 cm⁻¹ in Raman spectrum. V. Karunakaran et al.[24] in the molecule 4-chloro-3-nitrobenzaldehyde have observed the C–C stretching vibrations at 1589, 1356, 1200 and 1056 cm⁻¹ in FT-IR spectrum and at 1626, 1372, 1160 and 1058 cm⁻¹ in Raman spectrum.

The bands due to the C–C stretching vibrations are called skeletal vibrations normally observed in the region 1430–1650 cm⁻¹ for the aromatic ring compounds.[25, 26] Socrates [27] mentioned that the presence of a conjugate substituent such as C=C causes stretching of peaks around the region of 1625–1575 cm⁻¹. As predicted in the earlier references, in this title compound, the prominent peaks are found with strong and medium intensity at 1600 and 1590 cm⁻¹ due to C=C stretching vibrations. The C–C stretching vibrations have appeared at 1580, 1520, 1470 and 1400 cm⁻¹. The C-C out-of-plane bending vibrations have appeared at 1130, 1090, 1000 and 970 cm⁻¹.

C−N Vibrations

The C−N vibration of the compound identification is a very difficult task, since the mixing of several bands is possible in the region. Silverstein et al. [28] assigned C−N stretching absorption in the region 1382–1266 cm⁻¹ for aromatic amines. In benzamide the band observed at 1368 cm⁻¹ is assigned due to C−N stretching [29]. However with the help of force field calculations, the C−N vibrations are identified and assigned in this study. A. Prabakaran et al.[30] in 7-(1,3-dioxolan-2-ylmethyl)-1,3-dimethylpurine-2,6-dione (7DDMP26D) have observed C–N, C=N stretching vibrations at 1478.19 and 1280.19 cm⁻¹ in FT-IR spectrum and at 1480.00 and 1280.53 cm⁻¹ in FT-Raman spectrum respectively. In our present work, C−N stretching vibrations are observed at 1400 and 1180 cm⁻¹ in FT-IR spectrum. This band has been calculated at 1403 cm⁻¹ by DFT method and at 1180 cm⁻¹ by HF method are in very good agreement with experimental values.

C=O Vibrations

The C=O stretching frequency appears strongly in the IR spectrum in the range 1600–1850 cm⁻¹ because of its large change in dipole moment. The carbonyl group vibrations give rise to characteristics bands in vibration spectra and its characteristic frequency is used to study a wide range of compounds. The intensity

of these bands can increase owing to conjugation or formation of hydrogen bonds [31]. Carthigayan et al. [32] have observed the bands at 1822 and 1842 cm^{-1} in the infrared spectrum corresponding to C=O stretching in 4,5-Bis(bromomethyl)-1,3-dioxol-2-one (45BMDO). The corresponding frequency of 4-Bromomethyl-5-methyl-1, 3-dioxol-2-one (4BMDO) was observed at 1820 cm^{-1}. A very strong IR absorption band at 1680 cm^{-1} is readily assigned to the carbonyl vibration in the o-nitrobenzamide; the corresponding DFT computed mode at 1720 cm^{-1} at B3LYP/cc-pVDZ, level is in good agreement with the observed one.

NBO Analysis

The second order perturbation NBO Fock matrix was carried out to evaluate the donor–acceptor interactions in the NBO analysis. The interaction result is a loss of occupancy from the localized NBO of the idealized Lewis structure into an empty non-Lewis orbital. For each donor (i), and acceptor (j), the stabilization energy E$^{(2)}$ associated with the delocalization i→j is estimated as

$$E^2 = ΔE_{ij} = q_i \frac{F(i, j)^2}{\varepsilon_j - \varepsilon_i}$$

Natural bond orbital analysis provides an efficient method for studying intra and intermolecular bonding and interaction among bonds, and also provides a convenient basis for investigating charge transfer or conjugative interaction in molecular systems [33]. Some electron donor orbital, acceptor orbital and the interacting stabilization energy resulted from the second-order perturbation theory [34] are where q_i is the donor orbital occupancy, are ε_i and ε_j diagonal elements and F (i, j) is the off diagonal NBO Fock matrix element reported [35, 36]. The larger the E$^{(2)}$ value, the more intensive is the interaction between electron donors and electron acceptors, i.e. the more donating tendency from electron donors to electron acceptors the greater the extent of conjugation of the whole system [37]. Delocalization of electron density between occupied Lewis-type (bond or lone pair) NBO orbitals and formally unoccupied (anti-bond or Rydgberg) non- Lewis NBO orbitals correspond to a stabilizing donor–acceptor interaction. NBO analysis has been performed on the o-nitrobenzamide molecule in order to elucidate the delocalization of electron density within the molecule.

Table 4: Second Order Perturbation Theory Analysis of Fock Matrix in NBO Basis of O-Nitrobenzamide Using DFT/B3PW91/aug-cc-pVDZ Method

DONOR	BONDING	OCCUPANCY	ACCEPTOR	BONDING	OCCUPANCY	E(2) ^{a}Kcal/ mol	ENERGY DIFFERENCE^b E(j)-E(i) a.u	POLARISATION^c F(I,j) a.u
C1 – C2	σ	1.97259	C1 - C6	σ*	0.01561	2.19	1.31	0.048
C1 – C2	σ	1.97259	C1 – H7	σ*	0.01402	1.00	1.16	0.031
C1 – C2	σ	1.97259	C2 – C3	σ*	0.03055	5.03	1.31	0.073
C1 – C2	σ	1.97259	C3 – C11	σ*	0.07664	3.31	1.15	0.056
C1 – C2	σ	1.97259	C6 – H10	σ*	0.01331	2.44	1.17	0.048
C1 – C2	σ	1.97259	N16 – O18	σ*	0.06567	2.35	1.16	0.047
C1 – C2	π	1.64765	C3 – C4	π*	0.32605	21.84	0.30	0.073
C1 – C2	π	1.64765	C5 – C6	π*	0.31571	17.61	0.30	0.065
C1 – C2	π	1.64765	N16 – O17	π*	0.61356	24.54	0.15	0.058
C1 – C6	σ	1.97371	C1 – C2	σ*	0.02168	2.66	1.28	0.052
C1 – C6	σ	1.97371	C1 – H7	σ*	0.01402	1.16	1.15	0.033
C1 – C6	σ	1.97371	C2 – N16	σ*	0.10480	4.71	1.00	0.063
C1 – C6	σ	1.97371	C5 – C6	σ*	0.01634	2.20	1.29	0.048
C1 – C6	σ	1.97371	C5 – H9	σ*	0.01313	2.57	1.15	0.049
C1 – C6	σ	1.97371	C6 – H10	σ*	0.01331	0.79	1.15	0.027
C1 – H7	σ	1.97520	C1 – C2	σ*	0.02168	4.28	1.30	0.067
C1 – H7	σ	1.97520	C2 – C3	σ*	0.03055	3.21	1.30	0.058
C2 – C3	σ	1.96746	C1 – C2	σ*	0.02168	4.28	1.30	0.067
C2 – C3	σ	1.96746	C1 – H7	σ*	0.01402	2.01	1.17	0.043
C2 – C3	σ	1.96746	C3 – C4	σ*	0.02115	3.21	1.30	0.058
C2 – C3	σ	1.96746	C3 – C11	σ*	0.07664	1.87	1.15	0.042
C2 – C3	σ	1.96746	C4 – H8	σ*	0.01339	2.49	1.17	0.048
C2 – C3	σ	1.96746	C11 – N12	σ*	0.07227	0.66	1.20	0.025
C3 – C4	σ	1.96320	C2 – C3	σ*	0.03055	3.83	1.29	0.063
C3 – C4	σ	1.96320	C2 – N16	σ*	0.10480	5.13	1.00	0.065

C3 – C4	σ	1.96320	C3 – C11	σ*	0.07664	1.58	1.13	0.038
C3 – C4	σ	1.96320	C4 – C5	σ*	0.01578	2.25	1.29	0.048
C3 – C4	σ	1.96320	C4 – H8	σ*	0.01339	0.76	1.15	0.026
C3 – C4	σ	1.96320	C5 – H9	σ*	0.01313	2.29	1.15	0.046
C3 – C4	σ	1.96320	C11 – O15	σ*	0.06733	1.72	1.21	0.041
C3 – C4	π	1.64566	C1 – C2	π*	0.36828	20.80	0.28	0.069
C3 – C4	π	1.64566	C5 – C6	π*	0.31571	21.38	0.29	0.070
C3 – C11	σ	1.96681	C1 – C2	σ*	0.02168	3.42	1.22	0.058
C3 – C11	σ	1.96681	C2 – C3	σ*	0.03055	1.93	1.24	0.044
C3 – C11	σ	1.96681	C2 – N16	σ*	0.10480	0.51	0.94	0.020
C3 – C11	σ	1.96681	C3 – C4	σ*	0.02115	1.80	1.22	0.042
C3 – C11	σ	1.96681	C4 – C5	σ*	0.01578	3.14	1.23	0.056
C3 – C11	σ	1.96681	N12 – H13	σ*	0.01077	3.18	1.08	0.053
C4 – C5	σ	1.97703	C3 – C4	σ*	0.02115	2.64	1.28	0.052
C4 – C5	σ	1.97703	C3 – C11	σ*	0.07664	3.23	1.13	0.055
C4 – C5	σ	1.97703	C4 – H8	σ*	0.01339	0.98	1.15	0.030
C4 – C5	σ	1.97703	C5 – C6	σ*	0.01634	2.19	1.29	0.048
C4 – C5	σ	1.97703	C5 – H9	σ*	0.01313	0.79	1.15	0.027
C4 – C5	σ	1.97703	C6 – H10	σ*	0.01331	2.64	1.15	0.049
C4 – H8	σ	1.97861	C2 – C3	σ*	0.03055	4.70	1.11	0.065
C4 – H8	σ	1.97861	C5 – C6	σ*	0.01634	3.99	1.11	0.059
C5 – C6	σ	1.97843	C1 – C6	σ*	0.01561	2.21	1.30	0.048
C5 – C6	σ	1.97843	C1 – H7	σ*	0.01402	2.75	1.15	0.050
C5 – C6	σ	1.97843	C4 – C5	σ*	0.01578	2.19	1.29	0.048
C5 – C6	σ	1.97843	C4 – H8	σ*	0.01339	2.67	1.14	0.049
C5 – C6	σ	1.97843	C5 – H9	σ*	0.01313	0.82	1.15	0.027
C5 – C6	σ	1.97843	C6 – H10	σ*	0.01331	0.88	1.15	0.028
C5 – C6	π	1.63520	C1 – C2	π*	0.36828	23.46	0.28	0.073
C5 – C6	π	1.63520	C3 – C4	π*	0.32605	19.18	0.29	0.067
C5 – H9	σ	1.98059	C1 – C6	σ*	0.01561	3.99	1.11	0.060
C5 – H9	σ	1.98059	C3 – C4	σ*	0.02115	4.27	1.10	0.061
C5 – H9	σ	1.98059	C4 – C5	σ*	0.01578	0.62	1.11	0.023
C5 – H9	σ	1.98059	C5 – C6	σ*	0.01634	0.58	1.11	0.023
C6 – H10	σ	1.98073	C1 – C2	σ*	0.02168	4.01	1.10	0.059
C6 – H10	σ	1.98073	C4 – C5	σ*	0.01578	3.98	1.11	0.059
N12 – H13	σ	1.98514	C3 – C11	σ*	0.07664	4.52	1.07	0.063
N12 – H14	σ	1.98229	C11 – O15	σ*	0.06733	3.76	1.16	0.060
N16 – O17	π	1.98546	C1 – C2	π*	0.36828	3.06	0.47	0.037
N16 – O17	π	1.98546	N16 – O17	π*	0.61356	7.21	0.33	0.052
N12	n	1.75299	C11 – O15	σ*	0.06733	5.75	0.79	0.063
O15	n	1.97717	C3 – C11	σ*	0.07664	2.13	1.09	0.044
O15	n	1.97717	C11 – N12	σ*	0.07227	2.42	1.14	0.047
O15	n	1.84949	C3 – C4	π*	0.32605	0.95	0.26	0.015
O17	n	1.98106	C2 – N16	σ*	0.10480	4.42	1.10	0.064
O17	n	1.98106	N16 – O18	σ*	0.06567	2.59	1.24	0.051
O18	n	1.97978	C2 – N16	σ*	0.10480	4.71	1.10	0.066
O18	n	1.97978	N16 – O17	σ*	0.06130	2.03	1.24	0.045
O18	n	1.88917	C11 – O15	π*	0.22113	1.82	0.43	0.026
O18	n	1.88917	N16 – O17	π*	0.61356	1.13	0.17	0.014

LP – Lone pair.   [a] Stabilisation (delocalisation) energy.   [b] Energy difference between i(donor) and j(acceptor) NBO orbitals.   [c] Fock matrix element i and j NBO orbitals.

The intra molecular hyper conjugative interactions of π (C1–C2) to π* (N16–O17) leads to highest stabilization of 24.54 kcal mol^{-1}. In case of π (C1–C2) orbital the π*(C3–C4) shows the stabilization energy of 21.84 and 17.61 kcal mol^{-1}. Similarly in the case of   π (C3–C4) to π* (C1–C2) and π* (C5–C6) anti-bonding orbital leads to stabilization energy of 20.80 and 21.38 kcal mol^{-1} and from π (C5–C6) to π* (C1–C2), π*(C3–C4) has stabilization energies of 23.46 and 19.18 kcal mol^{-1}, respectively are listed in Table 4. The π – π* transition and corresponding perturbation energy are shown in figure 4.
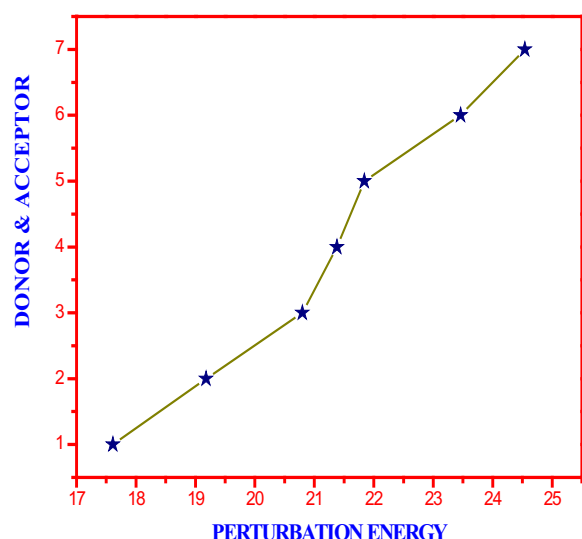
Note:
1=C1-C2→ C5-C6, 2=C5-C6 → C3-C4, 3=C3-C4→C1-C2, 4=C3-C4 →C5-C6, 5=C1-C2→ C3-C4, 6=C5-C6 →C1-C2, 7=C1-C2→ N16-O17

Figure 4: $\pi - \pi^*$ **Transition and Corresponding Perturbation Energy**

NMR Assessment

NMR spectroscopy is currently used for the structural elucidation of complex molecules. The combined use of experimental and computational tools offers a powerful gadget to interpret and predict the structure of bulky molecules. The optimized structure of o-nitrobenzamide is used to obtain the NMR spectra supported by the GIAO method with B3LYP functional at the cc-pVDZ basic set, and the chemical shifts of the compound are reported in ppm relative to TMS for ^{1}H and ^{13}C NMR spectra, which are presented in Table 5. The corresponding spectrum is shown in Fig. 5 & 6.

^{13}C NMR chemical shifts for similar organic molecules usually are >100 ppm [38, 39]. The accuracy ensures reliable interpretation of spectroscopic parameters. In the case of o-nitrobenzamide, the chemical shifts of C1, C2, C3, C4, C5, C6, and C11 are 132.429, 144.929, 122.479, 120.791, 118.984, 122.882 and 179.985 ppm respectively. The shift is higher in C2 and C11 than the others.

All the carbon atoms in the molecule are found to have higher chemical shifts due to the presence of highly negative atoms attached to the carbons. Among this C11 atom has higher chemical shift compared to all other atoms. It is due to attachment of electrons withdrawal amide carbonyl functional group.

The calculated values are compared with the experimental values. It is found that the calculated values are higher than the experimental values. And the lower peaks of hydrogen in experimental spectrum is found to be missing.

Table 5: Experimental and Calculated ^{1}H and ^{13}C NMR chemical shifts (ppm) of O-Nitrobenzamide

Atom position	Experimental Value (ppm)	Gas B3LYP/cc-pVDZ GIAO (ppm)	Solvent		
			Methanol B3LYP/cc-pVDZ GIAO (ppm)	Ethanol B3LYP/cc-pVDZ GIAO (ppm)	DMSO B3LYP/cc-pVDZ GIAO (ppm)
C1	133	132.429	133.586	133.564	133.608
C2	147	144.929	144.798	144.797	144.8
C3	131	122.479	122.946	122.94	122.952
C4	128	120.791	122.979	122.937	123.021
C5	123	118.984	122.424	122.366	122.481
C6	132	122.882	125.152	125.114	125.188
C11	168	179.985	182.813	182.769	182.855
7H	-	6.7288	6.7987	6.7978	6.7995
8H	8.2	8.5839	8.7702	8.7671	8.7733
9H	7.6	7.554	7.8743	7.8691	7.8794
10H	7.8	7.637	7.9422	7.9374	7.9468
13H	-	2.8879	3.1966	3.1932	3.1999
14H	-	2.1573	2.6503	2.6419	2.6586
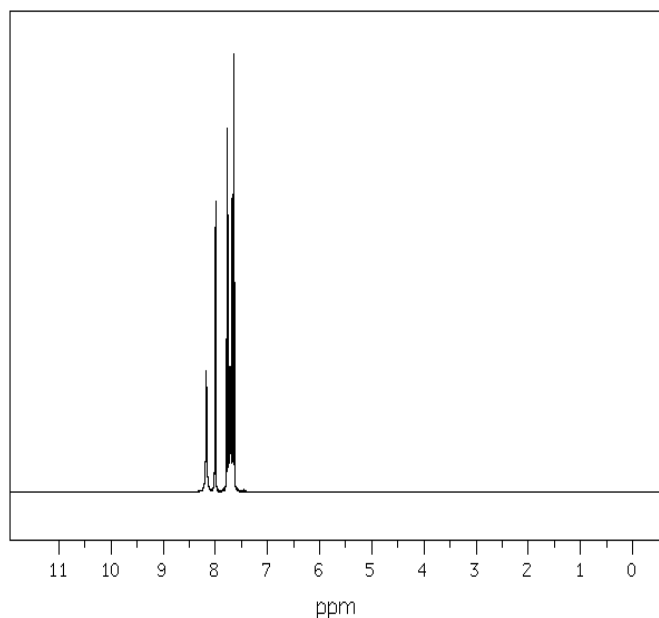
Figure 5: ¹H NMR Spectrum of O-Nitrobenzamide
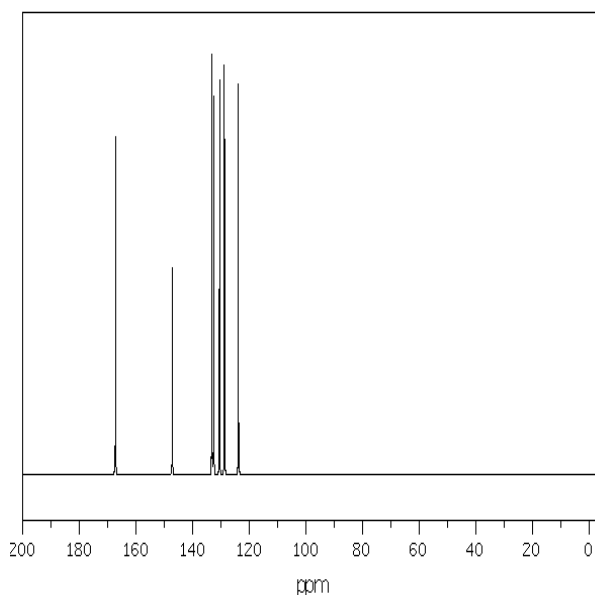
Figure 6: ¹³C NMR Spectrum of O-Nitrobenzamide

Electronic and Optical Properties (HOMO-LUMO Analysis)

UV-visible spectroscopy is used to detect the presence of chromophores in the molecule. The calculations of the electronic structure of o-nitrobenzamide have been optimized in the singlet state. The 3D plots of frontier orbitals for the molecule are shown in Fig. 7. The low energy electronic excited states of the molecule are calculated at the B3LYP/cc-pVDZ level using the TD-DFT approach based on the previously optimized ground-state geometry of the molecule. The calculations have been performed for o-nitrobenzamide in the gas phase and with the solvent of DMSO, ethanol, and methanol. The calculated excitation energies, oscillator strength (f), wavelength (λ) and spectral assignments are presented in Table 6.

Table 6: Theoretical electronic absorption spectra of O-Nitrobenzamide (absorption wavelength λ (nm), excitation energies E (eV) and oscillator strengths (f)) using TD-DFT/B3LYP/cc-pVDZ method

λ (nm)	E (eV)	(f)	Major contribution	Assignment	Region	Bands
Gas						
341.81	3.6273	0.0128	H→L (100%)	n→π*	Quartz UV	R-band
325.36	3.8106	0.0038	H→L (20%)	n→π*	Quartz UV	
289.07	4.2891	0.0030	H→L (15%)	n→π*	Quartz UV	(German, radikalartig)
DMSO						
337.04	3.6786	0.0174	H→L (80%)	n→π*	Quartz UV	R-band
318.58	3.8917	0.0087	H→L (40%)	n→π*	Quartz UV	
287.98	4.3053	0.0251	H→L (100%)	n→π*	Quartz UV	(German, radikalartig)
Ethanol						
337.15	3.6774	0.0169	H→L (80%)	n→π*	Quartz UV	R-band
318.75	3.8897	0.0082	H→L (40%)	n→π*	Quartz UV	
287.94	4.3059	0.0231	H→L (100%)	n→π*	Quartz UV	(German, radikalartig)
Methanol						
337.03	3.6787	0.0166	H→L (80%)	n→π*	Quartz UV	R-band
318.63	3.8912	0.0081	H→L (40%)	n→π*	Quartz UV	
287.90	4.3064	0.0229	H→L (95%)	n→π*	Quartz UV	(German, radikalartig)

H: HOMO; L: LUMO

HOMO

LUMO   (4.4113 eV)
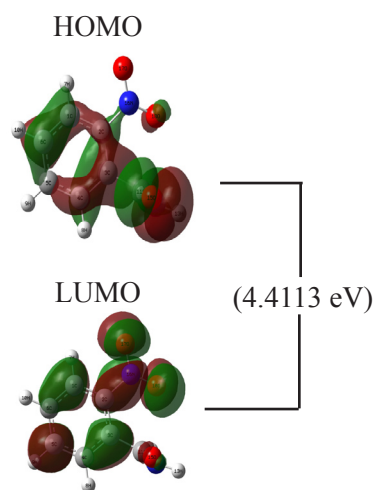
Figure 7: Frontier Molecular Orbitals of O-Nitrobenzamide

Figure 8: UV-Visible Spectrum of O-Nitrobenzamide

TD-DFT calculations predict three transitions in the quartz ultraviolet region. In the case of the gas phase, the strong transition is at 341.81, 325.36 and 289.07 nm with an oscillator strength of f = 0.0128, 0.0038, 0.0030 with 3.6273 eV energy gap. The transition is n→π* in the visible and the quartz ultraviolet region. The designation of the band is R-band (German, radikalartig) which is attributed to the above-said transition of amide groups. They are characterized by low molar absorptivities (ξ_{max}<100) and undergo a hypsochromic shift with an increase in the solvent polarity. The simulated UV-Visible spectrum of o-nitrobenzamide is shown in Fig. 8. The longer wavelengths observed on the UV spectra are due to transition from non-bonding lone pair's nitrogen and oxygen; they do have less frequency and higher perturbation energy.

In the case of the DMSO solvent, the strong transitions are obtained at 337.04, 318.58, 287.98 nm with an oscillator strength of f = 0.0174, 0.0087, 0.0251 and with a maximum energy gap of 3.6786 eV. They are assigned to n → π* transitions. This shows that, from the gas to the solvent phase, the transitions moved from the visible to the quartz ultraviolet region. This view indicates that the o-nitrobenzamide molecule has crystal property, and thus having rich NLO properties. In addition to that, the calculated optical band gap 4.4673 eV ensures that the present compound has NLO properties. In the view of calculated absorption spectra, the maximum absorption wavelength corresponds to the electronic transition from the HOMO to LUMO with maximum contribution.

Table 7: HOMO, LUMO, Kubo gap, global electronegativity, global hardness and softness, global electrophilicity index of O-Nitrobenzamide

Parameters	Gas	DMSO	Ethanol	Methanol
E_{HOMO} (eV)	-7.0167	-7.1383	-7.1340	-7.1361
E_{LUMO} (eV)	-2.6054	-2.6710	-2.6686	-2.6697
ΔE_{HOMO} - $E_{LUMO\ gap}$ (eV)	-4.4113	-4.4673	-4.4654	-4.4664
Chemical hardness(η)	2.2056	2.2336	2.2327	2.2332
Global softness(σ)	0.4533	0.4477	0.4478	0.4477
Electronegativity(χ)	4.8110	4.9046	4.9013	4.9029
Electrophilicity index(ω)	5.2469	5.3847	5.3797	5.3820

The chemical hardness, potential, electronegativity and electrophilicity index are calculated and their values are shown in Table 7. The chemical hardness is a good indicator of the chemical stability. The chemical hardness increased slightly (2.205–2.233 eV) in going from the gas to the solvent phase. Hence, the present

compound has high chemical stability. Similarly, the electronegativity is observed to have increased from 4.8 to 4.9 eV. The electrophilicity index is a measure of energy lowering due to the maximal electron flow between the donor [HOMO] and the acceptor [LUMO]. From Table 7, it is found that the electrophilicity index

of o-nitrobenzamide is 5.2469 eV in the gas phase and 5.3847 eV in solvent phase, which is moderate, and this value ensures the energy transformation between HOMO and LUMO. The dipole moment in a molecule is another important electronic property. Whenever the molecule has larger dipole moment, the intermolecular interactions are very strong. The calculated dipole moment value for the title compound is 4.9575 D in the gas phase and 6.2624 D in the solvent phase. It is high, which shows that the o-nitrobenzamide molecule has strong intermolecular interactions.

Global Softness and Local Region Selectivity

Molecular charge distribution, molecular orbital surfaces, HOMO and LUMO energies have been used as reactivity descriptors in the DFT study. The energy gap between the HOMO and LUMO orbitals has been found to be adequate to study the stability and chemical reactivity of a great variety of molecular systems and is an important stability index. Besides the traditional reactivity descriptors, there are a set of chemical reactivity descriptors that can be derived from DFT, such as global hardness (η), global softness, local softness (S), Fukui function (f), global and local electrophilicity indexes (ω).[40–50] These quantities are often defined by Koopman's theorem.[51,52]

Electronegativity (χ) is the measure of the power of an electron or a group of atoms to attract electrons towards it [53] and according to Koopman's theorem, it can be estimated using the following equation:

$$\chi = -\frac{1}{2}(E_{Homo} + E_{Lumo}) \tag{1}$$

where E_{Homo} is the energy of the highest occupied molecular orbital (HOMO) and E_{Lumo} is the energy of the lowest unoccupied molecular orbital (LUMO). Global hardness (η) measures the resistance of an atom to a charge transfer [54] and it is estimated using the equation:

$$\eta = -\frac{1}{2}(E_{Homo} - E_{Lumo}) \tag{2}$$

Global softness (S) describes the capacity of an atom or a group of atoms to receive electrons [55] and it is estimated using the equation:

$$S = \frac{1}{\eta} = -2(E_{Homo} - E_{Lumo}) \tag{3}$$

where η is the global hardness values. The global electrophilicity index (ω) is estimated using the electronegativity and chemical hardness parameters through the equation:

$$\omega = \frac{\chi}{2\eta} \tag{4}$$

A high value of electrophilicity describes a good electrophile, while a small value of electrophilicity describes a good nucleophile.

Table 8: Fukui Function and Global and Local Softness and Electrophilicity Index of O-Nitrobenzamide

Atom	f+ = (q+1)-q	f- = q-(q-1)	Δf = (f+)-(f-)	ΔS =Δfσ$_{gs}$	Δω=Δfω$_{gei}$
1C	0.029098	0.016798	0.012300	0.00557559	0.0645381
2C	0.001077	0.006884	-0.005807	-0.00263231	-0.030469329
3C	0.003745	0.005696	-0.001951	-0.00088439	-0.010236897
4C	0.026440	0.021234	0.005206	0.00235988	0.027315882
5C	0.039029	0.031642	0.007387	0.00334853	0.038759589
6C	0.027700	0.022167	0.005533	0.00250811	0.029031651
7H	0.042211	0.054621	-0.012410	-0.00562545	-0.06511527
8H	0.047403	0.055193	-0.007790	-0.00353121	-0.04087413
9H	0.059105	0.064098	-0.004993	-0.00226333	-0.026198271
10H	0.055008	0.061720	-0.006712	-0.00304255	-0.035217864
11C	0.062395	0.055484	0.006911	0.00313276	0.036262017
12N	0.067579	0.012124	0.055455	0.02513775	0.290972385
13H	0.046722	0.035364	0.011358	0.00514858	0.059595426
14H	0.045745	0.031938	0.013807	0.00625871	0.072445329
15O	0.095817	0.011028	0.084789	0.03843504	0.444889982
16N	0.003696	0.059376	-0.055680	-0.02523974	-0.29215296
17O	0.185714	0.221245	-0.035531	-0.0161062	-0.186431157
18O	0.161491	0.233389	-0.071898	-0.03259136	-0.377248806

ΔS = local softness, σ$_{gs}$ = global softness; Δω = local electrophilic index, ω$_{gei}$ = global electrophilic index.

Fukui indices is a measure of the chemical reactivity, as well as an indicator of the reactive regions and the nucleophilic and electrophilic behaviors of the molecule. The regions of a molecule, where the Fukui function is large, are chemically softer than the regions where the Fukui function is small, and by invoking the HSAB principle in a local sense, one may establish the behavior of different sites with respect to hard or soft reagents. The Condensed to atom Fukui function is a reactive descriptor to identify nucleophilic and electrophilic attack sites in candidate molecules; perhaps it is also used to recognize the electron acceptor center and donor centers. If $fk+$ for any given site is positive then it is a preferred site for nucleophilic attack, in contrast the negative value implies electrophilic attack.

The Fukui function is defined as [56, 57]:

$$f(r) = \left(\frac{\partial \rho(r)}{\delta N}\right)_{v(r)} \tag{5}$$

Where $\rho(r)$ is the electron density and

$$N = \int \rho(r)\mathrm{dr} \tag{6}$$

Where N is the number of electrons and r is the external potential exerted by the nucleus.

The phenyl ring gets activated at the *ortho* and *para* positions as there are electron releasing substituents such as –OH, –NH$_2$, –OR, R, etc. A propyl substituent in fact is an electron releasing substituent, consequently promotes the *ortho* and *para* positions for electrophilic attack, a common reactivity trend observed in phenyl compounds. Local reactivity descriptors such as $fk+$, $fk-$, Δf, ΔS and $\Delta\omega$ for the different sites of the phenyl ring are in conformity with the observed reactivity trend of the candidate molecule. The values are shown in Table 8.

$fk+$, $fk-$, Δf, ΔS and $\Delta\omega$ unambiguously reveal the order of the nucleophilic attack to be in the decreasing sequence as C1 > C5 > C11>C6>C4 and that of the electrophilic attack is found to be C3 > C2 in the phenyl ring. This trend for the attack of the electrophile is in conformity with that of ΔS and $\Delta\omega$. The atoms C2, C3 are more prone to nucleophilic attack and C1, C5 are more favorable to electrophilic attack. The *ortho* and *para* positions show the tendency for attack of the electrophile, which is indeed a common trend observed in alkyl substituted phenyl ring compounds. The different charges of atoms are plotted and shown in the fig. 9 & 10.
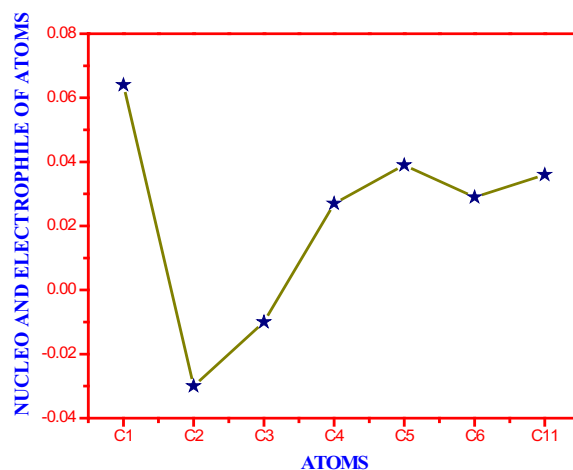

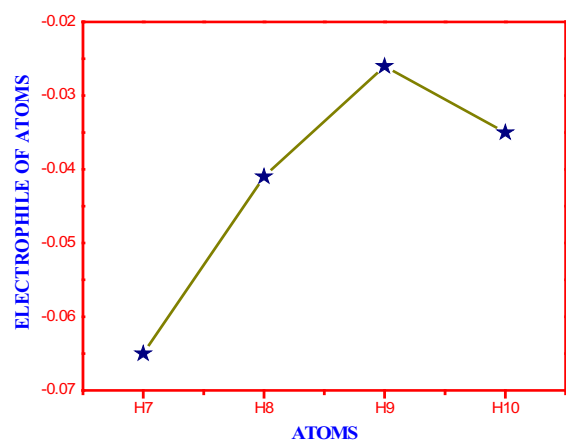**Figure 9: Positively & Negatively Charged Atoms of O-Nitrobenzamide Using Fukui Function**

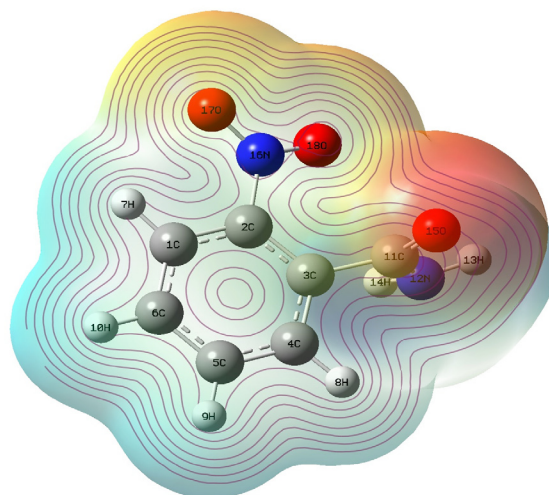**Figure 10: Negatively Charged Atoms ofO-Nitrobenzamide Using Fukui function**

Figure 11: MEP Contour Map of O-Nitrobenzamide

Molecular Electrostatic Potential (MEP) Maps

The molecular electrical potential surfaces, as shown in Fig. 11, illustrate the charge distributions of molecules three dimensionally. This map allows visualizing variably charged regions of a molecule. The knowledge of the charge distributions can be used to determine how molecules interact with one another and it is also used to determine the nature of the chemical bond. Molecular electrostatic potential is calculated at the B3LYP/cc-pVDZ optimized geometry. [58, 59] There is a great deal of intermediary potential energy, and the non-red or blue regions indicate that the electro negativity difference is not very great. In a molecule with a great electro negativity difference, charge is very polarized, and there are significant differences in electron density in different regions of the molecule. This great electro negativity difference leads to regions that are almost entirely red and almost entirely blue. [60] The Greater regions of intermediary potential, yellow and green, and smaller or no regions of extreme potential, red and blue, are key indicators of smaller electronegativity.

The color code of these maps is in the range between −5.490 a.u. (deepest red) and 5.490 a.u. (deepest blue) in the compound. The positive (blue) regions of MEP are related to electrophilic reactivity and the negative (green) regions to nucleophilic reactivity (Fig. 11). From the MEP map of the candidate molecule, it can be observed that the red regions of the molecule were found to be ready for electrophilic attack, and especially in the phenyl ring the atoms are clouded with red color. From the findings of the Fukui local reactivity descriptor, it can be observed that the atoms C1, C4, C5, C6 and C11 are nucleophiles ready for electrophilic attack and atoms C2 and C3 are the regions for nucleophilic

attack. The molecular electrostatic potential map can be confirmed with the finding of the Fukui descriptors.

Polarizability and First Order Hyperpolarizability Calculations

In order to investigate the relationships among molecular structures and non-linear optic properties (NLO), the polarizabilities and first order hyperpolarizabilities of the o-nitrobenzamide compound were calculated using the DFT-B3LYP method and the cc-pVDZ basis set, based on the finite-field approach.

The polarizability and hyperpolarizability tensors $(\alpha_{xx}, \alpha_{xy}, \alpha_{yy}, \alpha_{xz}, \alpha_{yz}, \alpha_{zz}$ and $\beta_{xxx}, \beta_{xxy}, \beta_{xyy}, \beta_{yyy}, \beta_{xxz}, \beta_{xyz}, \beta_{yyz}, \beta_{xzz}, \beta_{yzz}, \beta_{zzz})$ can be obtained by a frequency job output file of Gaussian. However, α and β values of the Gaussian output are in atomic units (a.u.); so they have been converted into electronic units (esu) (α, 1 a.u. $= 0.1482\times10^{-24}$ esu; β, 1 a.u. $= 8.6393\times10^{-33}$ esu). The calculations of the total molecular dipole moment (μ), linear polarizability (α) and first-order hyperpolarizability (β) from the Gaussian output have been explained in detail previously,[61,62] and DFT has been extensively used as an effective method to investigate the organic NLO materials.[63–67]

$$\alpha_{tot} = \frac{1}{3}(\alpha_{XX} + \alpha_{YY} + \alpha_{ZZ})$$

$$\Delta a = \frac{1}{\sqrt{2}}\left[\begin{array}{l}\left(\alpha_{xx} - \alpha_{yy}\right)^2 + \left(\alpha_{yy} - \alpha_{zz}\right)^2 \\ + \left(\alpha_{zz} - \alpha_{xx}\right)^2 + 6\alpha^2_{xz} + 6\alpha^2_{xy} + 6\alpha^2_{yz}\end{array}\right]^{\frac{1}{2}}$$

$$\langle\beta\rangle = \left[\begin{array}{l}\left(\beta_{xxx} + \beta_{xyy} + \beta_{xzz}\right)^2 + \left(\beta_{yyy} + \beta_{yzz} + \beta_{yxx}\right)^2 \\ + \left(\beta_{zzz} + \beta_{zxx} + \beta_{zyy}\right)^2\end{array}\right]^{\frac{1}{2}}$$

Table 9: The electronic dipole moment (μ) (Debye), polarizability (α) and first hyperpolarizability (β) of O-Nitrobenzamide

Parameter	a.u.	Parameter	a.u.
α_{xx}	-55.5541	β_{xxx}	-36.4230
α_{xy}	5.2440	β_{xxy}	7.8514
α_{yy}	-71.4564	β_{xyy}	1.0538
α_{xz}	3.4014	β_{yyy}	19.7313
α_{yz}	0.1110	β_{xxz}	-3.0686
α_{zz}	-69.7811	β_{xyz}	3.2892
α_{tot}	-65.5972	β_{yyz}	-1.6681
$\Delta\alpha$	13.1587	β_{xzz}	-10.9696
μ_x	-1.9888	β_{yzz}	-7.4288
μ_y	- 5.7088	β_{zzz}	-1.9797
μ_z	-0.9490	β_{tot}	50.9762
μ_{tot}	6.1193		

In Table 9, the calculated parameters described above and the electronic dipole moment $\{\mu_i \ (i = x, y, z)\}$ and total dipole moment μ_{tot} for the title compound are listed. The total dipole moment is calculated using the following equation: [68]

$$\mu_{tot} = \left(\mu^2_x + \mu^2_y + \mu^2_z \right)^{\frac{1}{2}}$$

It is well known that the molecules with high values of dipole moment, molecular polarizability, and first hyperpolarizability have more active NLO properties. The first hyperpolarizability *(β)* and the components of hyperpolarizability α_x, α_y and α_z of o-nitrobenzamide along with related properties *(α_0, α_{total}, and $\Delta\alpha$)* are reported in Table 8. The calculated value of the dipole moment is found to be 6.1193 D. The highest value of the dipole moment is observed for component μ_Z which is equal to −0.9490 D and the lowest value of the dipole moment of the molecule for the component μ_Y is −5.7088 D. The calculated average polarizability and anisotropy of the polarizability is −9.721x10^{-24} esu and 1.950x10^{-24} esu, respectively. The magnitude of the molecular hyperpolarizability is one of the important key factors in an NLO system. The B3LYP/cc-pVDZ calculated first hyperpolarizability value (β) is 4.404x10^{-35} esu. From the above results, it is observed that, the molecular polarizability and hyperpolarizability of the title compound in all coordinates are active. So that o-nitrobenzamide can be considered to the good candidate for NLO material.

Conclusion

In the geometrical study, it is observed by the calculation of the bond length and bond angle, the hexagonal structure of the compound is deformed. In the vibrational study though most of the vibrations are in line with the literature some the mode carbonyl group is shifted to the end position of the range. The NMR reveals that the C11 atom which is attached to the carbonyl and amine group has more shift compared to all other atoms in the compound; it means that atom is more deshielded by its electrons. From the UV steady it is found that the π and nonbonding orbital transitions have almost occurred in the spectra. From the range of the wavelength it is observed that the transition entered into the visible blue range. Thus it is a good candidate of the NLO material. From the MEP mapping and Fukui study the possible electrophile and nucleophile have been identified.

References

1. R.J. Knox, M.P. Boland, F. Friedlos, B. Coles, C. Southan, J.J. Roberts, Biochemical Pharmacology, 37 (1988) 4671–4677.

2. A. Chandor, S. Dijols, B. Ramassamy, Y. Frapart, D. Mansuy, D. Stuehr, N. Helsby, Chemical Research Toxicology, (2008), 21, 836–843.

3. R.J. Lewis, Sr (Ed.). Hawley's Condensed Chemical Dictionary, 12th ed. New York, NY: Van Nostrand Rheinhold Co., (1993) 860.

4. D. Hartley and H. Kidd (eds.), The Agrochemicals Handbook. Old Woking, Surrey, United Kingdom: Royal Society of Chemistry/Unwin Brothers Ltd., (1983).

5. W. Gerhartz, Ullmann's Encyclopedia of Industrial Chemistry. 5th ed: Deerfield Beach, FL: VCH Publishers, 1985.

6. M.K. Marchewka, A. Pietraszko, Spectrochimica Acta Part A, 69 (2008) 312– 318.

7. M.J. Frisch, Gaussian 09, Revision A.02, Gaussian, Inc., Wallingford CT, 2009.

8. Z. Zhengyu, D. Dongmei, Journal of Molecular Structure, 505 (2000) 247-252.

9. Z. Zhengyu, F. Aiping, D. Dongmei, Journal of Quantum Chemistry, 78 (2000)   186-189.

10. A.D. Becke, Physics Review A, 38 (1988) 3098-3101.

11. C. Lee, W. Yang, R.G. Parr, Physics Review B, 37 (1988) 785-790.

12. A.D. Becke, Journal of Chemical Physics, 98 (1993) 5648-5652.

13. R.L. Peesole, L.D. Shield, I.C. McWilliam, Modern Methods of Chemical Analysis, Wiley, New York, 1976.

14. S. Mohan, N. Sundaraganesan, J. Mink, Spectrochim. Acta A, 47 (1991) 1111–1115.

15. G.N. Ten, V.V. Nechaev, A.N. Pankratov, V.I. Berezin, V.I. Baranov, *Journal* of Structural *Chemistry*, 51 (2010) 854–861.

16. V. Arjunan, S. Sakiladevi, T. Rani, C.V. Mythili, S. Mohan, Spectrochimica Acta Part A, 88 (2012) 220–231

17. C. Cırak, N. Koc, Journal of Molecular Modeling, 18 (2012) 4453–4464.

18. N.P.C. Roeges, A Guide to the Complete Interpretation of Infrared Spectra of Organic Structure, Wiley, New York, USA, 1994.

19. Y.R. Sharma, Elementary Organic Spectroscopy, Principles and Chemical Applications, S.Chande & Company Ltd., New Delhi, 1994.

20. P.S. Kalsi, Spectroscopy of Organic Compounds, Wiley Eastern Limited, New Delhi, 1993.

21. V. Karunakaran, V. Balachandran, Spectrochimica Acta Part A: Molecular and Biomolecular Spectroscopy, 98 (2012) 229 –239.

22. V. Arjunan, K. Carthigayan, S. Periandy, K. Balamurugan, S. Mohan, Spectrochimica Acta Part A: Molecular and Biomolecular Spectroscopy, 98 (2012) 156–169.

23. V. Arjunan, K. Carthigayan, S. Periandy, K. Balamurugan, S. Mohan, Spectrochimica Acta Part A: Molecular and Biomolecular Spectroscopy, 98 (2012) 156–169.

24. V. Karunakaran, V. Balachandran, Spectrochimica Acta Part A: Molecular and Biomolecular Spectroscopy, 98 (2012) 229–239.

25. M. Silverstein, G. Clayton Basseler, C. Morrill, Spectrometric identification of organic Compounds, John Wiley, New York, 1991.

26. C. Brian Smith, Infrared Spectral Interpretation, CRC Press, New York, 1999.

27. G. Socrates, Infrared and Raman Characteristics Group Frequencies, Wiley, New York, 2000.

28. M. Silverstein, G. Clayton Basseler, C. Morill, Spectrometric Identification of Organic Compound, Wiley, New York, 1981.

29. R. Shanmugam, D. Sathyanarayana, Spectrochim. Acta A, 40 (1984) 764.

30. A. Prabakaran, S. Muthu, Spectrochimica Acta Part A: Molecular and Biomolecular Spectroscopy, 118 (2014) 578–588.

31. R. Zhang, X. Li, X. Zhang, Frontiers of Chemistry in China, 6 (2011) 358-366.

32. K. Carthigayan, V. Arjunan, R. Anitha, S. Periandy, S. Mohan, Journal of Molecular Structure, 1056 (2014) 38–51.

33. S. Subhashandrabose, R. Akhil, R. Krishnan, H. Saleem, R. Parameswari, N. Sundaraganesan, V. Thanikachalam, G. Manikandan, Spectrochim. Acta, 77A (2010) 877–884.

34. J.N. Liu, Z.R. Chen, S.F. Yuan, Journal of Zhejiang University-Science B, 6 (2005) 584–589.

35. C. James, A. Amalraj, A. Regunathan, V.S. Jayakumar, I.H. Joe, Journal of Raman Spectroscopy, 37 (2006) 1381–1392.

36. A.R. Krishanan, H. Saleem, S. Subhashandrabose, N. Sundaraganesan, S. Sebastian, Spectrochimica. Acta A, 78 (2011) 582–589.

37. S. Sebastian, N. Sundaraganesan, Specrochim. Acta, A 75 (2010) 941–952.

38. J.H. Vander Maas and E.T.G. Lutz, Spectrochimica Acta, A 30 (1974) 2005.

39. S. Ahmad, S. Mathew, P.K. Verma, Indian Journal of Pure and Applied Physics, 30 (1992) 764-770.

40. R.G. Parr, W. Yang, Density Functional Theory of Atoms and Molecules, Oxford University Press, New York, 1989.

41. P. Geerlings, F. De Proft, W. Langenaekar, Advanced Quantum Chemistry, 33(1999) 303-332.

42. K. Hohenberg, W. Kohn, Physical Review, 136 (1964) B864.

43. R.G. Pearson, Journal of American Chemical Society, 85 (1963) 3533-3539.

44. R.G. Parr, R.G. Pearson, Journal of American Chemical Society, 105 (1983) 7512-7516.

45. R.G. Parr, R.A. Donnelly, M. Levy, W.E. Palke, Journal of Chemical Physics, 68 (1978) 3801-3807.

46. R.G. Pearson, Journal of American Chemical Society, 107 (1985) 6801-6806.

47. R.G. Parr, W. Yang, Journal of American Chemical Society, 106 (1984) 4049-4059.

48. R.G. Parr, L.V. Szentpaly, S. Liu, Journal of American Chemical Society, 121 (1999) 1922-1924.

49. P. Perez, A. Toro-Labbe, A. Aizman, R. Contreras, Journal of Organic Chemistry, 67 (2002) 4747-4752.

50. W. Yang, W. Mortier, Journal of American Chemical Society, 108 (1986) 5708-5711.

51. P. Geerlings, F. De Proft, W. Langenaeker, Chem. Rev. 103 (2003) 1793-1874.

52. R.G. Parr, R.G. Pearson, Journal of American Chemical Society, 105 (1983) 7512-7516.

53. L. Pauling, The Nature of the Chemical Bond (Coruell University Press, Ithaca, New York, 1960.

54. R.G. Parr, R.G. Pearson, Journal of American Chemical Society, 105 (1983) 7512-7516.

55. R.G. Parr, W. Yang, Functional Theory of Atoms and Molecules, Oxford University Press, New York, 1989.

56. P.W. Ayers, R.G. Parr, Journal of American Chemical Society, 122 (2000) 2010-2018.

57. R.G. Parr, W. Yang, Journal of American Chemical Society, 106(1984) 4048- 4049.

58. M. Nendel, K.N. Houk, L.M. Tolbert, E. Vogel, H. Jiao, P.V.R. Schleyer, Journal of Physical Chemistry. A, 102 (1998) 7191-7198.

59. C.H. Choi, M. Kertesz, Journal of Chemical Physics, 108 (1998) 6681-6688.

60. A. Vektatiene, Journal of Organic Chemistry, 26 (2009) 321-322.

61. H. Tanak, Y. Köysal, H. Yaman, V. Ahsen, Bulletin of Korean Chemical Society, 32 (2011) 678-686.

62. K.S.Thanthiriwatte, K.M. Nalin de Silva, Journal of Molecular Structure (Theochem) 617 (2002) 169-175.

63. Y.X. Sun, Q.L. Hao, Z.X. Yu, W.X. Wei, L.D. Lu, X. Wang, Molecular Physics, 107 (2009) 107, 223-235.

64. A.B. Ahmed, H. Feki, Y. Abid, H. Boughzala, C. Minot, A. Mlayah, Journal of Molecular Structure, 920 (2009) 1-4.

65. J.P. Abraham, D. Sajan, V. Shettigar, S.M. Dharmaprakash, I. Nemec, I.H. Joe, V.S. Jayakumar, Journal of Molecular Structure, 917 (2009) 27-36.

66. S.G. Sagdinc, A. Esme, Spectrochimica Acta Part A, 75 (2010) 1370-1376.

67. A.B. Ahmed, H. Feki, Y. Abid, H. Boughzala, C. Minot, Spectrochimica Acta Part A, 75 (2010) 293-298.

68. Y.J. Jiang, Chinese Science Bulletin, 57 (2012) 4449-4453.